PRECISION MEASUREMENTS OF ^{20}F BETA DECAY

By

Maximilian Nathan Hughes

A DISSERTATION

Submitted to
Michigan State University
in partial fulfillment of the requirements
for the degree of

2018

ABSTRACT

PRECISION MEASUREMENTS OF ^{20}F BETA DECAY

By

Maximilian Nathan Hughes

TABLE OF CONTENTS

Chapter 1

Introduction

Precision measurements at low energy can compete with high energy measurements.

1.1 Beta Decay

Beta decay is cool and good.

Chapter 2

Theoretical Description of Beta Decay Spectrum

To obtain a measure of the Fierz term, the beta decay spectrum must be precisely described. The description of the beta decay spectrum is writen as a series of corrections on top of the main phase space factor.

The corrections depend on several parameters of the decay. Some of them are just numbers, such as the atomic number of the daughter or mother nucleus or the mass number of the system. However, there are two important paramters that are inexact. They are measured experimentally.

One is the q-value of the decay, which is defined in equation 3.1.

$$Q = m_p - (m_d + E_\gamma) \tag{2.1}$$

where Q is the q-value, m_p is the mass of the parent nucleus, m_d is the mass of the daughter nucleus, and E_γ is the energy of any gamma rays in the decay. For this measurement, the atomic mass of ^{20}Ne and ^{20}F were used [8]. The mass of the electrons subtracts out atomic masses, since in neutral fluorine there are nine electrons, and one electron is gained from the beta decay. This then equals the ten electrons in the atomic mass of neon. The only correction missing is the small, eV scale electron binding energy of the last electron.

The other parameter is the charge radius of the daughter nucleus. There are several ways to calculate the charge radius. In this work, the charge radius was taken from the measured RMS charge radius and converted. It was assumed that the ^{20}Ne nucleus was a sphere. From this, the radius was calculated using equation 2.2

$$r = \sqrt{\frac{5}{3}} r_{rms} \tag{2.2}$$

where r_{rms} is the root mean square radius, and r the charge radius.

With the two parameters, the q-value and the phase space, the shape of all beta decay spectra can be described.

2.1 Phase Space Beta Decay

The main part of the beta decay spectrum is the phase space factor. It is shown in equation 2.3

$$\frac{dN}{dE} = C * p_\beta W (Q - W)^2 \tag{2.3}$$

were C is a constant, p_β is the beta momentum, W the total electron energy, and Q the q-value of the beta decay. This is derived from the density of states of the particle. This comes in from Fermi's Golden Rule.

The number of states for both the electron and the neutrino is show in equation 2.4

$$N = \frac{1}{(2\pi\hbar)^6} \int dr_\beta^3 \int dp_\beta^3 \int dr_{\nu e}^3 \int dp_{\nu e}^3 \tag{2.4}$$

where r and p corresponds to the position and momentum of the electron (β) and the

neutrino (ν_e). Doing the integral over both r's give two factors of the volume, which disappear when the next factor is introduced. Since the neutrinos are unmeasured, the momentum of the neutrinos is integrated over. Assuming spherical symmetry, the new integral is shown in equation 2.5

$$dN = \frac{V^2}{4\pi^4\hbar^6}p_\beta^2 dp_\beta p_{\nu_e}^2 dp_{\nu_e} \tag{2.5}$$

This is simplfied by approximating the neutrino as massless. The momentum of the neutrino is then equal to the energy of the neutrino. Then, the total energy E is written as a sum of the neutrino energy (or momemntum) and the beta energy. Plugging that in gives equation 2.6 after integrating over the neutrino degrees of freedom.

$$dN = \frac{V^2}{4\pi^4\hbar^6}(E - E_{beta})^2 p_\beta^2 dp_\beta \tag{2.6}$$

Then, the only thing left to do to recover equation 2.3 is to rewrite dp in terms of dE. The energy E_{beta} has been replaced with W, which is the energy of the electron divided by the mass an electron, and E has been replaced by the Q-value. Since the measurement is not an absolute one, but only concerned with the shape of the spectrum, the normalization factor is arbitrary.

This is the main factor in describing the beta decay energy spectrum.

2.2   Variables of Correction Formula

For the rest of the discussion on beta decay corrections, everything is given without units. All of the energies are divided by the electron mass, i.e. 511 keV. The other important

variables are shown in table **??**

Variable	Description	Equation or Value
A	Mass number	20
Z	Atomic number of daughter	10
α	Fine structure constant	1/137.0359
R	Root mean square charge radius of daughter	3.055 fm [2]
W	Total energy of beta electron	E/m_e
p	Electron momentum	$\sqrt{W^2 - 1}$
E_0	Maximum electron energy	$\frac{M_{20_F} - M_{20_{Ne}} - E_{gammaray}}{m_e}$
γ	Factor that shows up in EM corrections	$\sqrt{1 - (\alpha Z)^2}$

To convert the RMS charge radius into the regular charge radius, it is assumed that the nucleus was a sphere. This means multiplying the radius given in table **??** by $\sqrt{\frac{3}{5}}$. Finally, in order to put it into natural units, the result was divided by the reduced Compton wavelength of the electron.

2.3 Fermi Function

The first correction is the Fermi function. This accounts for the interaction of the charge of the outgoing electron and the charge of the nucleus. It is calculated by taking the Dirac equation wave functions and assuming the nucleus is a point charge of Ze. The Dirac wave functions are taken down to a nuclear radius R. This is since the wave functions diverge [**?**].

The Fermi function is printed in equation 2.7

$$F(Z, W) = 2\frac{\gamma + 1}{\Gamma(2\gamma + 1)^2}(2pR)^{2(\gamma - 1)}e^{\frac{\pi \alpha Z W}{p}}\|\Gamma(\gamma + i\frac{\alpha Z W}{p}\|^2 \tag{2.7}$$

2.4 Radiative Correction

2.4.1 Inner Bremmsstrahlung

Chapter 3

^{20}F

In this measurement, the nucleus used was ^{20}F. The decay scheme is given in figure 3.1.
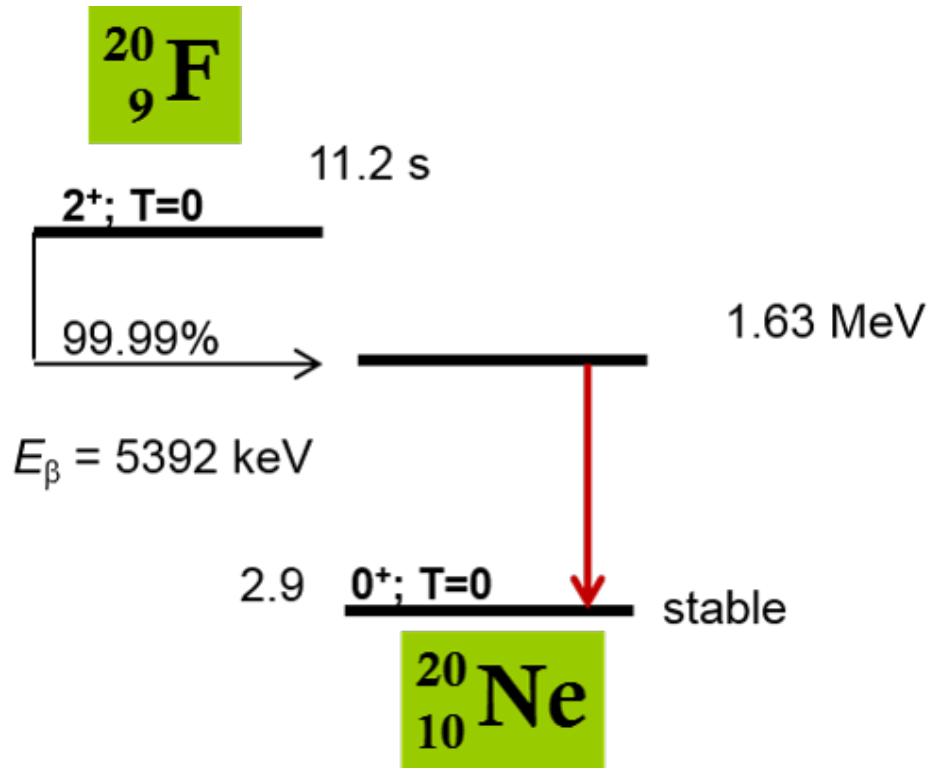
Figure 3.1: The decay scheme of ^{20}F.

As seen in the figure, ^{20}F decays 99.999% of the time to the first excited state of ^{20}Ne.

3.1 Theory Parameters

For the q-value of the decay, the atomic masses of ^{20}Ne and ^{20}F were used. The decay of ^{20}F of interest decays to an excited state of the ^{20}Ne. The energy of the gamma ray was

measured to 0.015 keV [9].

Using the numbers described above and equation 3.1, the q-value for ^{20}F is 5.901928 (82). The largest source of uncertainty is in the mass of ^{20}F.

$$Q = m_{^{20}F} - (m_{^{20}Na} + E_\gamma) \tag{3.1}$$

Chapter 4

Experimental Description

To measure the ^{20}F beta decay spectrum, a beam of ^{20}F was implanted into one of two different detectors. The isotope was implanted deeply enough from so that the detector material could completely absorb the energy of electron at the end point energy. The implantation of the beam was done to avoid instrumental effects of a non-calorimetry experiment. If there is a dead layer, there is more detector behind the layer to absorb the energy. The electron cannot scatter out of the detector.

The experiment was run at the National Superconducting Cyclotron Laboratory (NSCL) in East Lansing, Michigan. The detector set up is describe below.

4.1   Detector Set Up

4.1.1 ^{20}F Decay Detectors

One scintillator was a 3 in diameter by 3 in long cylinder of EJ-200 polyvinyltoluene (PVT). It was attached to a clear plastic disk attached to a photomultiplier tube. The idea was to avoid a rate dependent gain effect that was seen in a previous experiment. The plastic detector signal is fast (around 100 ns) which makes pile-up a lesser concern. This detector was built by colaborators for this experiment. During the experiment the voltage on the PMT of this scintillator was varied. This was due do an observed distortion in the beta

decay spectrum. A gain montitoring system was installed.

To monitor the gain of the plastic detector, a plastic disk containing an optical fiber was placed between the crystal and the photomultiplier tube. The other end of the fiber was fed into a box with an LED driven by a function generator. The box was made light-tight with electrical tape and black paint. An additional optical fiber fed the light to a Si PIN diode. This was to monitor the light output of the LED.

To help check for systematics effects, another implant detector was used. It was a 2 in by 2 in by 4 in CsI(Na) detector. This detector was a module from the CAESAR array [12]. It does not have any gain monitoring like the PVT detector, but it is similar to a detector used in a different experiment. The other experiment was a similar measurement with ^{6}He instead of ^{20}F.

In order to measure the gamma ray from the ^{20}F decay, a frame was built to hold four cubic 3 in CsI(Na) detectors. These were also part of the CAESAR array. The frame to hold the four detectors was designed to be able to move the four outer detectors around in various configurations. However, no other configurations were used during the experiment.

A sketch of both detector configurations is shown in Figure 4.1.

To switch between different implant detectors, the central detector in the frame was removed and put on the floor. The other detector was placed in the center of the four gamma detectors. The PVT detector was supported on a metal rail, while the CsI (Na) detector was supported on pile of scrap aluminum. Both of the detectors had the active scintillator part free in between the four large gamma detectors.
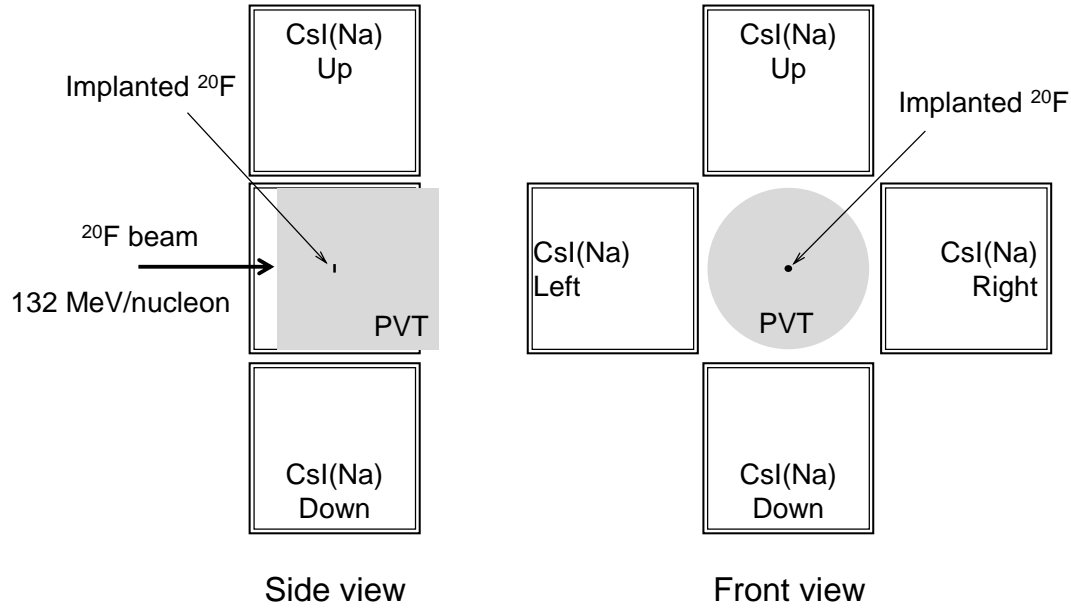
Figure 4.1: A sketch of the detector set up. Shown here is with the PVT detector implant. The CsI (Na) detector was centered in the middle of the the four gamma detectors and recessed by 1 inch. The bottom image shows a side of the detector set-up.

4.1.2 Other detectors

The light from the LED was also piped to a PIN diode. This was to get an independent measure of the light from the LEDs. A parrallel plate avalanch counter (PPAC) was used for beams size measurements. A Si detector was used to check the beam purity. A pulser was used to make sure the data acquisition clock was stable.

4.1.3 Powering the Detectors

To power the gamma and implant scintillators, 3 2-channel NHQ 212M ISEG power supplies were used. The Si detector was powered by a Tennelec TC248 amplifier. The PPAC was powered by an integrated power supply.

Each detector had a different voltage. The PVT implant detector was varied in voltage over the course of the experiment. This was due to concerns about saturation effects. Ini-

tially, the high voltage on the PVT detector was chosen to take advantage of the dynamic range of the detector. For the PPAC, The voltage for the four gamma detectors was chosen so that they had roughly the same gain. The voltages of the detectors is shown in table **??**.

Detector	HV (V)
PVT Implant (Sets 1-4)	-975
PVT Implant (Set 5)	-856
PVT Implant (Set 6)	-780
CsI (Na) Implant	780
CsI (Na) Gamma 1	930
CsI (Na) Gamma 2	1000
CsI (Na) Gamma 3	970
CsI (Na) Gamma 4	1015
Si Pin	20
Pin diode	15
PPAC	560

4.2   Beam

4.2.1   Beam Discription

The primary beam of ^{22}Ne was accelerated by the coupled cyclotrons to 150 MeV/A. A typical intensity of the primary beam was around $60 * 10^{-5}$pnA. It was impinged on a Be target and sent through the fragment separator. The resulting ^{20}F beam was at an energy of 130 MeV/A. The intensity of the ^{20}F was about $2 * 10^{-5}$ pnA, and the purity was about 93% at the end of the fragment separator.

4.2.2   Beam Size and Location

To test the size of the beam, a parralel plate avalanche counter was used. The size of the detector was 10 cm by 10 cm square. It was placed 65 cm upstream of the target. A

horizontal and verticle grid was in the detector. Depending on where on each of the grids the particles hit, different charges were sent to either end of the PPAC. The signals were fed into a digital data acquisition system, and read out as an energy. The difference of the two signals divided by the sum was interpretted as a position.

To calibrate the detector, a mask with several holes was used. This mask covered the front of the detector, and an alpha source in the vacuum was placed in front of the PPAC. Then, everything was left to run until an image of the mask was formed. The mask had holes in it every 1 cm. It also had a large L shaped hole so that the orientation of the mask could be seen. With this, the PPAC could be calibrated.

Before taking data for the beta decay spectrum measurement, the PPAC was inserted into the beam. After adjusting the parameters of the upstream beam optics, the final beam size at the PPAC was measured. The calibrated data of the signals was built into a 3-D histogram. There was some ringing in the PPAC, so the peak of the beam spot was fitted with a 3-D gaussian function. The average of the gaussian and the sigma in the x and y direction was taken. From the sigmas, the half widths at half maximum (HWHM) in both directions were calculated. The distribution of the locations were sampled at eight different points. The points are shown as the black dots in Fig: 4.2. They are one HWHM away from the center.

After averaging the 8 points, the range on the z axis was taken from the average of those points to the top. The resulting beam was measured to be 8 mm by 6 mm large.

This is the size of the spot at the PPAC. Ion optics simulations were used to build the cross section of the beam at the PPAC and at the target. Using these cross sections, the magnification between the two locations was calculated. The magnification was different between the x and y directions. Using the magnification, the X and Y beam size was found
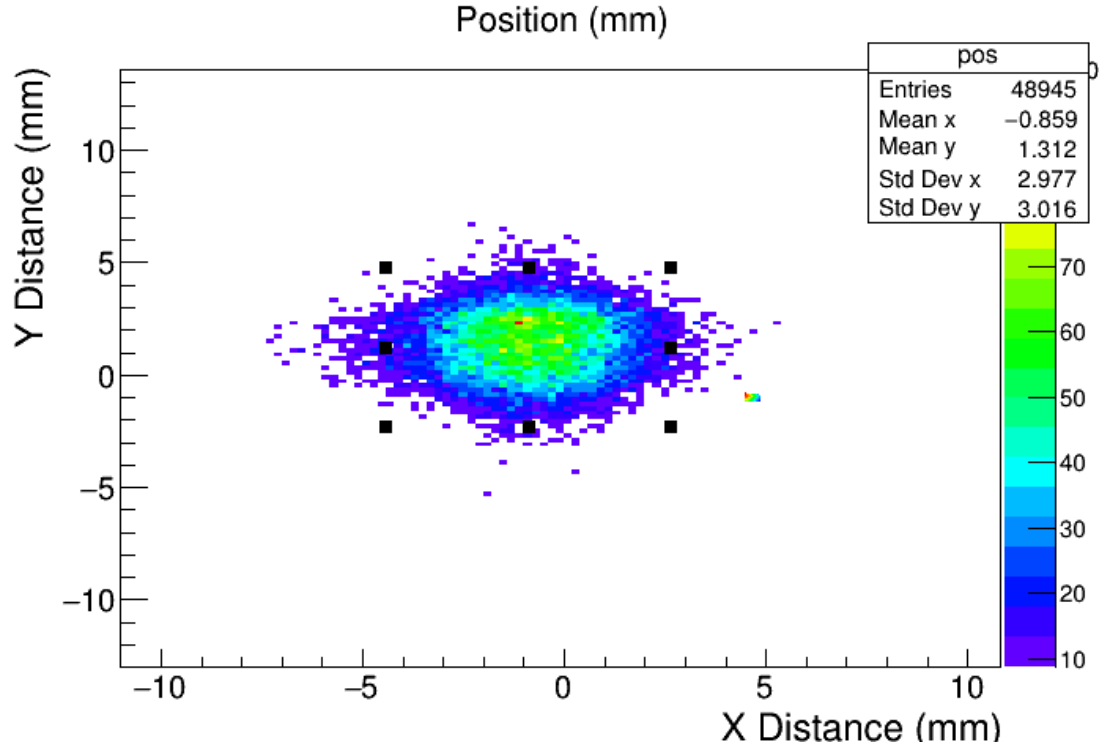
Figure 4.2: The beam spot of the calibrated PPAC spectrum. The samples of the spectrum that were averaged together are shown in the black dots. The center of the fit is not shown.

to be 3.6 mm by 3.4 mm.

For the depth of the implantation of the beam, ion simulations were used. The LISE++ program was fed the beam meagnets. It was given the energy of the beam and the detector set up. It then calculated the depth of the implantation of the detector and the range of the depth inside the detector. This gave a depth of 3.02 cm in side the PVT detector and a depth of 1.156 cm in the CsI(Na) detector. The range of the depth was 1.2 mm in the PVT detector and 0.4 mm in the CsI(Na) detector.

4.2.2.1   Beam Purity

The beam was filtered by S800 spectrograph. The purity measured there was at 93%, with the main contaminates being ^{18}O and ^{19}O. This was measured up stream of the detector set

14

up.

To double check the beam purity, two detectors were used. One was a thin Si PIN detector that was used as a δE detector. The other detector was a small CsI(Na) detector similar to the implant detector that was used during the steering and during the beam size measurement. It had a much lower voltage than the one used for the implantation measurement. Both of these in tandem were used to build a particle identification plot. From this, it was found that the beam is very clean.

4.2.3 Beam Implantation Depth

In order to verify the simulations for the beam implant depth, a degrader was inserted into the beam for a beam depth measurement. The degrader was made of aluminum and had two different thicknesses: 7.89 mm and 11.38 mm. The beam was caught by a CsI(Na) scintillator of a similar design to the one used for the implantation measurement. The angle of the degrader was changed to change the effective thickness of aluminum that the beam had to travel through. By varying this thickness to the one predicted to stop the beam out side of the detector, the depth of implantion could be verified. This was done after the main run, and the simulations proved to be correct.

4.3 Experimental Conditions

The data was taken in runs of roughly one hour. However, many runs where cut short when the DAQ stopped recording data for one of the detectors. In order to properly measure the decay, the beam was pulsed with an implantation time of anywhere from 1 to 2 seconds, and a decay time ranging from 22 s to 32 s. The beam was turned off since the light from the

implantation of the beam would drown out any signal obtained. A run with a decay time of 60 seconds was also taken for each implant detector.

To achieve the beam pulsing, two timer boxes were used. A CAEN N1145 quad scaler module was used to control the beam off time. This module had a digital control of time down to 1 ms. Once the the time finished counting down, a signal was sent to a second module. A CAEN N93B dual timer used the signal from the quad scaler as a start signal. The time period was set using a dial, which was less precise. Once the dual timer finished its time, it sent a signal back to the quad scaler to restart the cycle. The output of these two modules created a signal with one voltage level durinng the dual timer's time and another voltage condition during the quad scaler's time. This signal was fed into a box. The voltage level during the quad scaler's time dephased the cyclotron RF, turning the beam off. When the dual timer voltage level occured, the RF returned to the tuned value, turning the beam on.

After the frist couple of runs with the PVT detector, a high-voltage inhibitor box was installed. It was discovered that during the implantation period, a large amount of current was drawn by the PVT detector's PMT. There were also instabilities seen in the gain directly after beam on period. The inhibitor box does cause the gain during the beam on period to be very small, but that information is ignored. Any decay that happens during that period is swamped by the light produced by the beam imlpanting.

For the CsI(Na) runs, a current limit on the power supplies was enabled. It has a similar effect to the inhibitor box.

Chapter 5

Data Processing

The detector were tested using an oscilliscope to check for their signals. The signals were then inserted into a digital data acqusition system.

5.1   Data acquisiton

All the signals for all the detectors were sent to digitizers. These digitizers were three 250 mega-samples per second 16 channel XIA PIXIE modules. They were run with the digital NSCL system. The first module had the implant detectors and the four gamma detectors. The second module had five signals from the PPAC and one signal for the Si dector. Both of these had the beam on signal, beam off signal, a 100 Hz pulser, and the signal from the PIN photodiode. The third module only recorded the digitized waveforms from the PVT detector.

Each of the channels on each of those modules outputted a time stamp and an energy calculated from a trapezoidal fitler. The third module output the digitized waveform over 400ns. The clock used was a stable EPSON SGR-8002JC programmable crystal oscillator.

The first thing the PIXIE modules did was to digitize the wave forms of the signals. The digital wave forms of the signals were only saved for the PVT implant detector. The PIXIE modules' software applied a trapezoidal energy filter to the digital wave froms. The parameters of the trapezoidal needed to be set by hand. There was also a trigger filter in

the PIXIE system.

5.1.1 Data Acquisition Sofware

In order to set the parameters of the various filters, a program called NSCOPE was used
[**?**] The program GUI was used to set the rise time, the gap, and the threshold for both the
energy filter and the trigger filter. These parameters were set differently for each detector
type. The CsI(Na) detectors (the implant and the 4 gamma detectors) shared the rise time
and gap time, while other detectors had different parameters. Sample spectra were taken
with NSCOPE, and the parameters saved to a file.

This file was loaded with a program called ReadOut, which ran the data taking. The
ReadOut program used a ringbuffer in order to record the output of the data. The program
recorded data as an .evt binary file if the record data button was checked.

The ringbuffer was also fed to a program called scalers. This gave the rates of the events
coming into each channel. It gave an input rate to each channel, the recorded rate, and the
total over each run. This was to check how each channel in each module was doing.

For online analysis, a program called SpecTcl was used. It took the evt files and pro-
cessed them into histograms. These histograms could be put in coincidence. Displays of the
implant detector energy and rate were displayed. The energy of the implant vs time was
also displayed. Additionally, the implant energy vs time since last beam on was plotted as
a 2-D spectra. The decay curves (time in implant minus last beam on) were also plotted.
These histograms were used as diagnostics.

5.2 Data Taking and Processing

To take data, the ReadOut program was activated. Data was taken in one hour intervals, unless one of the detectors stopped counting early If a detector stopped early, it was the up detector. The run was then ended early and then a new one resarted.

The resulting .evt files of ReadOut were processed using a program called DDAS dumper. This converted the .evt files to ROOT files. These ROOT files contained a TTRee that had the energy and time stamps of each detector. There was also information on the trace of the detector.

From the ROOT files from the ddasdumper, another ROOT file was built. These files were processed with a code called scan, which was written by Stan Paulauskas. First, the various energies and times for each detector were built into a histogram. Then, the energy and times for the implant detectors, four gamma detectors, beam on signal, and beam off signals were saved to a variable. This information was used to build new events for a new TTree.

Each event started with a non-zero energy reading in any of the five detectors. Then, a 400 ns long time gate opened, during which all energies and times were saved into the event. The time signatures of the last beam on and beam off signals were also saved into each event. The energies of the beam on or beam off signals were 0 or 1.

Chapter 6

Half Life Measurement

6.1 Motivation

During the experiment, it was noticed that there was a disagreement between different values of the half-life. As a side project and as a chance to thoroughly investigate the data, a half-life measurement was taken. The prevous measurements of the half-life of ^{20}F are shown in Figure 6.1.
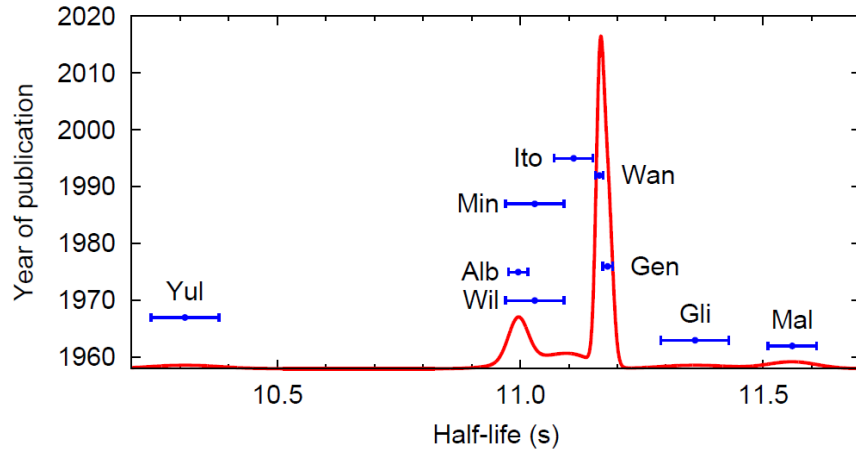

Figure 6.1: Previous measurements of the ^{20}F half-life. The labels correspond to: Mal [6], Gli [4], Yul [14], Wil [13], Alb [1], Gen [3], Min [7], Wan [11] and Ito [5].

This ideogram has a red line which is a sum of Gaussian functions. The centroids of the Gaussians are the central values of the measurements. The sigmas are the errors, and each gaussian is weighted by $\frac{1}{\sigma^2}$. This is to see that there are two different values that the half-lives are converging to.

20

It has been used in the past for searches of second-class currents and in astrophysics.

6.2 Half life data analysis

First, the data was processed as described in the previous chapter.

6.2.1 Data Selection

Only the data from the PVT impantation set was used for the half-life analysis. The rate depedent gain effect causes a large systematic effect in the CsI(Na) data. This effect causes the gain at early times is higher than the gain at later times in the decay cycle. The cuts, however, stay in the same position. Early in the decay cycle, events near the cuts could start out inside the window. As time goes on and the gain changes, these cuts could move below the lower beta cut. Due to the shape of the beta spectrum, the higher the lower beta cut, the larger the effect. This effect is seen in Figure 6.2.
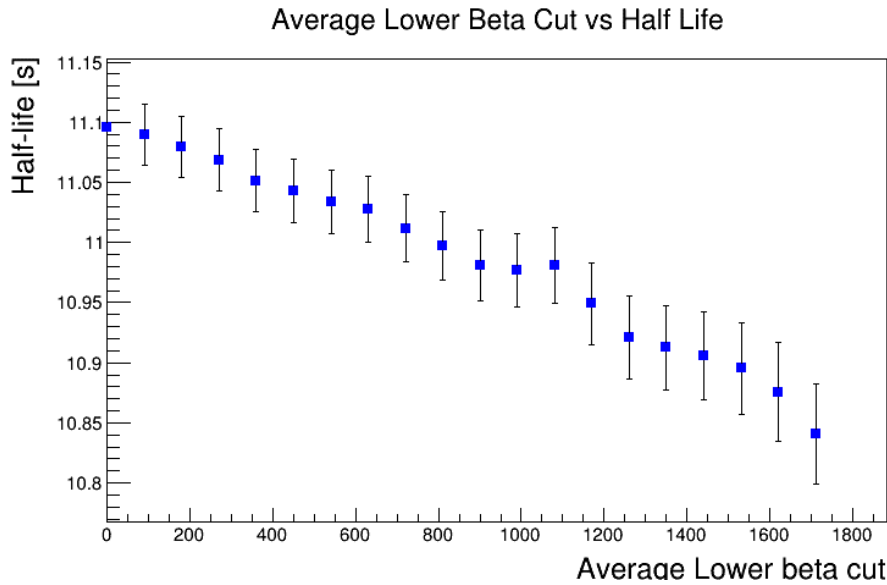

Figure 6.2: The effect of the lower beta cut vs the half-life in the CsI(Na) data

Attempts were made to counteract this effect with a more sophisticated analysis. The beta spectrum was built and fitted second by second in order to obtain a time-dependent calibration. The gain of the calibration was plotted as a function of time and fit with a line. The offest of the calibration was seen to be independent of time. The resulting time-dependent calibration was used to analyze the data. This reduced the effect seen in Figure 6.2, but did not entirely eliminate it. Since the CsI(Na) data has a small statistical impact, it was decided to elliminate that data from the analysis of the half-life. The cause of the rate dependent gain effect is afterglow in the CsI (Na) scintillator. The plastic scintllator does not have any afterglow, so the PVT implant detector is immune to this effect.

The PVT data was seperated into 7 sets. A summary of the set conditions is shown in Table 6.1 As shown in the table, the major conditions were the PVT high voltage, the inhibitor box, and the beam current.

Table 6.1: The PVT runs

Set	Beam on Time [s]	Measuring Time [s]	PVT HV [v]	HV Inhibit Installed	Beam intensity [nA]	Runs
1	1.67	30	-975	No	30	9
2	1.67	30	-975	No	93	2
3	1.67	30	-975	Yes	30	9
4	1.67	30	-975	Yes	93	11
5	1.67	30	-856	Yes	30	93
6	1.00	60	-800	Yes	93	1
7	1.10	20	-780	Yes	93	10

The inhibitor box was not installed until the third set of data. Without it, a time-dependent gain shift over the fitting window was induced. This time-dependent gain shift caused large systematic errors when the beta cuts were moved. Thus, sets 1 and 2 where not used in the final analysis. These gain shifts can be seen in Figure 6.3.
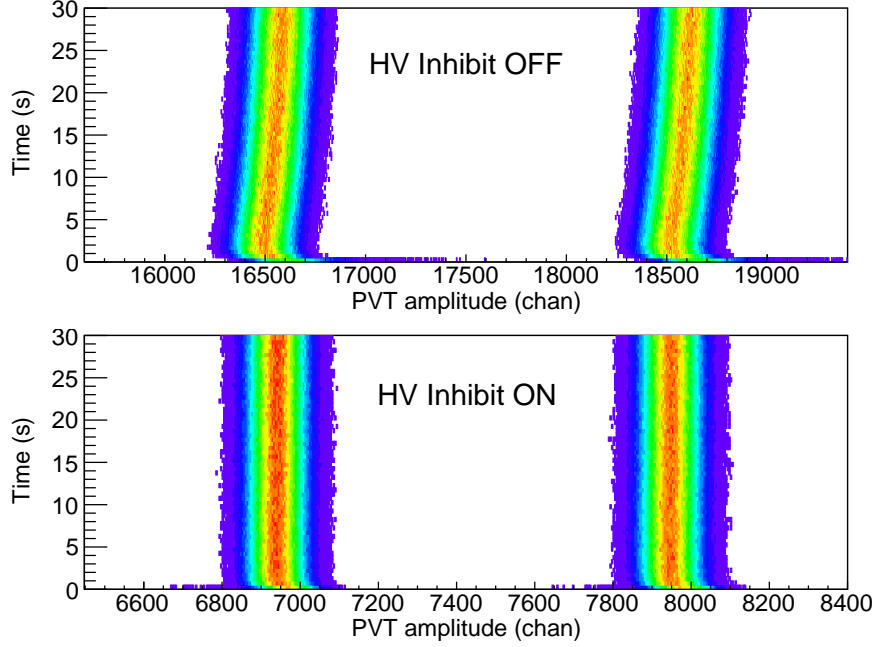
Figure 6.3: The light pulse as a function of time for set 1. The gain changes smoothly over time. This causes a large change in the half-life as the beta cuts are moved.

6.2.2 Cut Selection

In order to do the half-life analysis, software coincidences were imposed. Three conditions were set in total. Two conditions were on the energy in the implantation detector and one of the four CsI(Na) detectors. An additional condition on the time difference between the events recorded in the two detectors. A sample spectrum of all the gamma and beta energies is shown in Figure 6.4

Hard coded gates were used for to select in the beta window for the PVT run sets. Each different data set had a different energy window due to the gain shifts. A sample spectrum with the gates can be seen in Figure 6.5. This spectrum is put in coincidence with the gamma spectra. The lower beta cut was selected to cut out the 511 beta spectram as seen in Figure 6.4. When gated around that energies, the resulting gammas measured by the large CsI(Na) detectors are consistent with ^{10}C and ^{11}C. This comes from the break-up of the
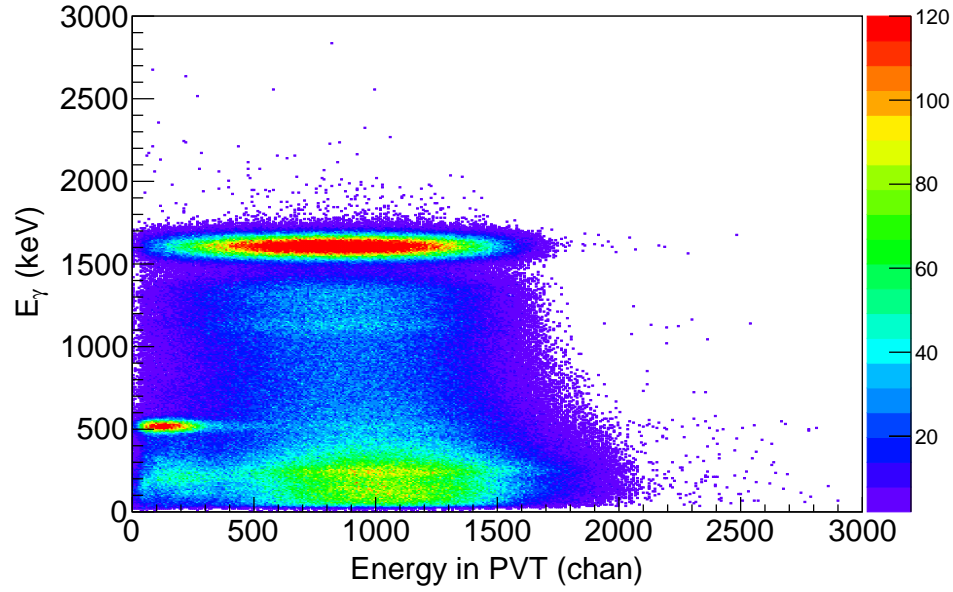
23

Figure 6.4: The 511 region can be seen in this graph

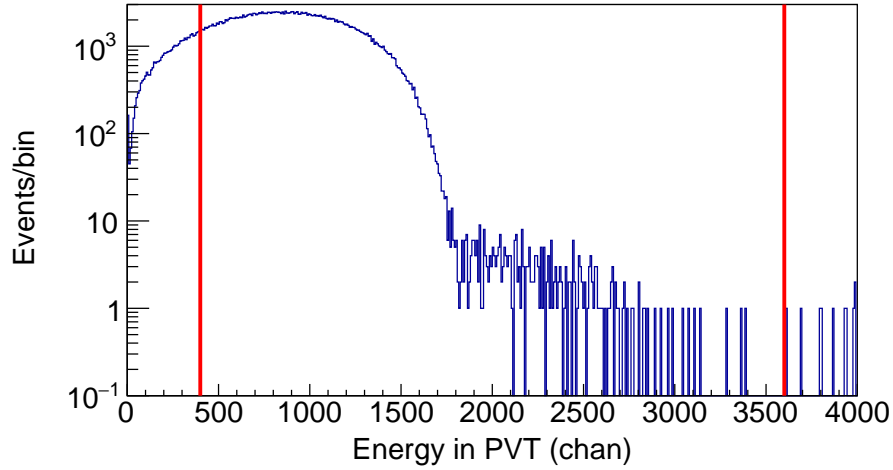Figure 6.5: The lower beta cut was selected to be above the 511 region. The upper beta cut was selected to include all the pile up

plastic.

The set of runs before the limiter box was installed have a gain shift within each run, similar to the rate dependent gain effect. This causes the half-life to vary greatly with the beta cut. As the beta gates are moved, different counts move across it over the time interval,
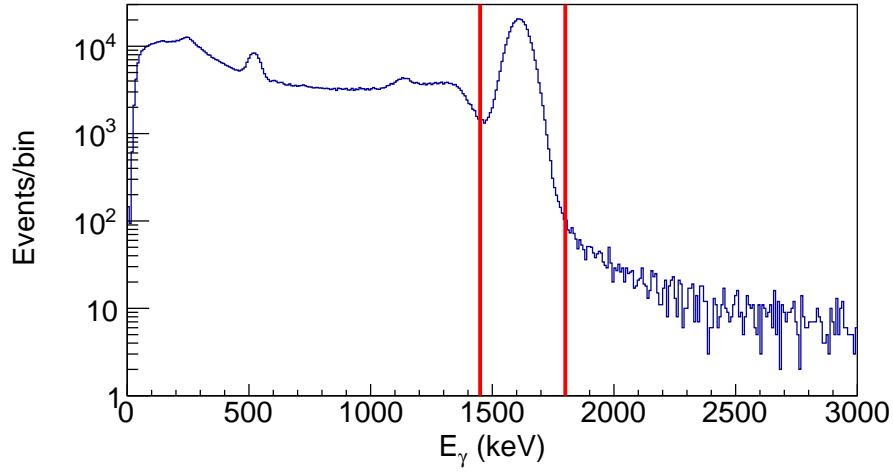
Figure 6.6: The wide cuts are to reduce the effect of the rate dependent gain.

causing a change in lifetime. Only the runs after the installation of the limiter box were used for the half-life analysis. This excluded the first and second sets of data.

A time difference condition was set by building a spectrum of the time differences between the implant detector's event and one of the four gamma detector's events. The peak of this time difference spectrum was found, and an interval of ± 24 ns was use for this gate. A sample time difference spectrum can be seen in Figure 6.7

The time differnce spectrum shows several features. First is the prompt peak, which are correlated gamma and beta events. To the right of the prompt peak, there is a pedistal of events. These come from pile-up events. What happens is that a ^{20}F event decays and the time stamp of the emmitted beta is recorded. The corresponding gamma ray is not detected. Then, within the pile-up window, a second ^{20}F decays. The implant detector is dead and does not record the second time stamp. Due to pile-up, the time stamp of the second beta event is not recorded. The gamma ray is then detected at a later time compared to the first event. An cartoon sketch of this effect is shown in Figure 6.8. The pedistal can be seen in full in Figure 6.9.
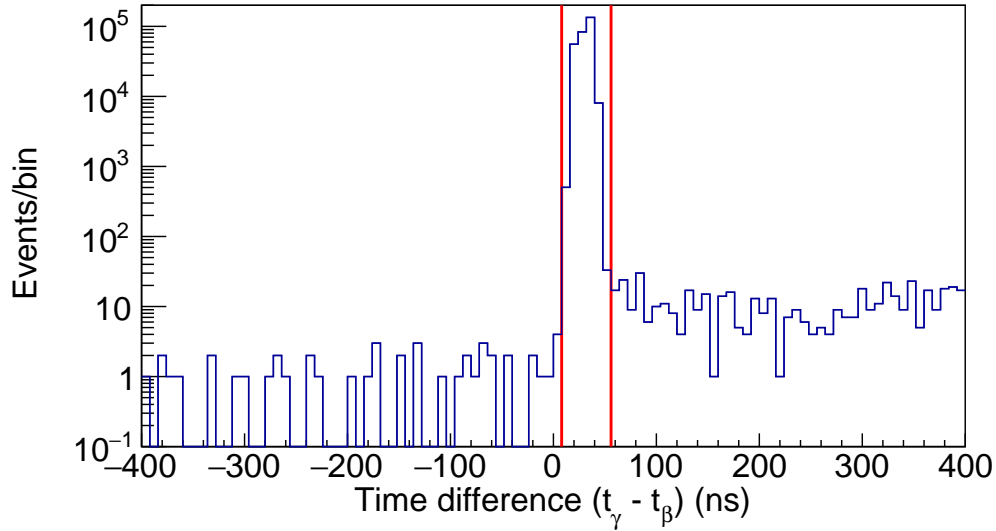
Figure 6.7: This is a gamma and beta energy filted spectrum of the time difference between the up detector and the PVT implant detector. The tail on the right side of the large peak is due to pile up. The narrow time cuts are shown with a dotted line. The wide time cuts are shown with a solid line.

The other events to the left of the prompt peak and to the right of the pile-up pedistal are accidental coincidences. These include the background coincidences.

The time signals for the outer four gamma detectors were used for the half-life analysis. This gave 4 independent measurements of the half-life per run. Only full decay cycles were used. This was done by finding the last beam on and putting a condition on the run time of the events. The decays where the up detector stopped counting were ignored, as there were few enough that they did not make a difference.

The dead time was corrected using measured rates and a dead time of 464 ns for the implant detector and 656 ns for the gamma detectors. The dead time was measured by building a spectrum of the time difference between consecutive time stamps. The lowest time difference was taken as the dead time. This was checked using the light pulser in the PVT detector. For each gamma detector, a histogram of the energy-filtered rate was built.
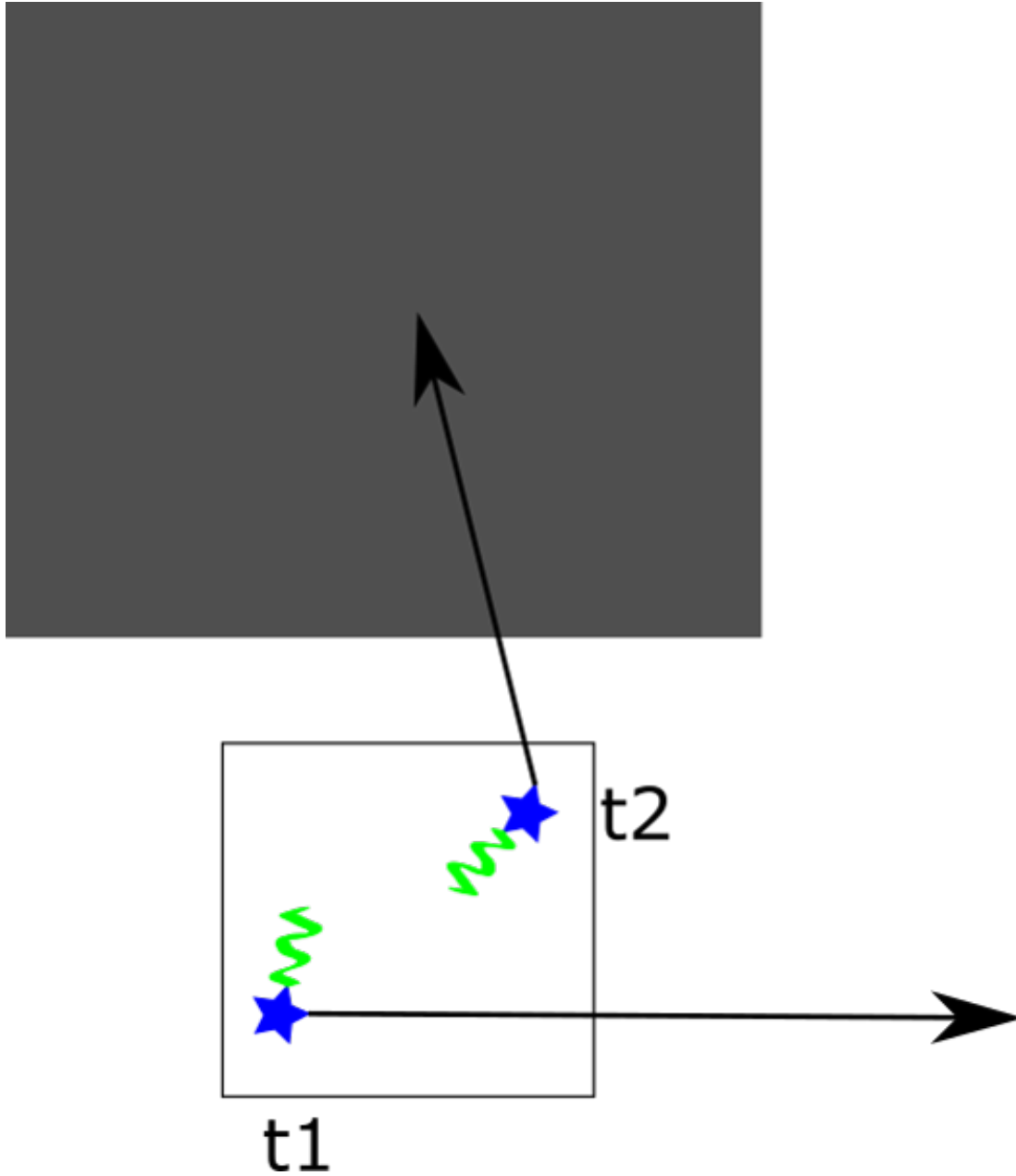
Figure 6.8: A sketch of the pile up events. A ^{20}F decay happens at time = t1. The green electron is detected in the implant detector. The black arrow (the gamma raw) is not. Then, later at time = t2, another ^{20}F decays. t2 is within the pile-up window of t1. Both electrons energies pile-up and are added together. However, the time stamp recorded by the DAQ is still t1. The gamma ray from event t2 can be detected in a gamma detector at time t2. This creates the uncorrelated event pedistal in the time difference graph.

Figure 6.9: The time difference spectrum zoomed out. There is still a gamma and beta energy conditions on this graph.

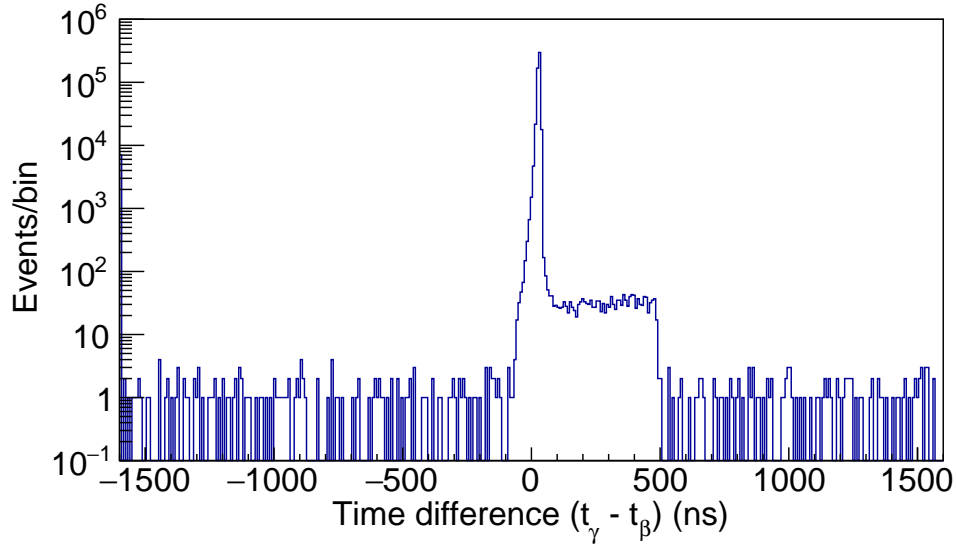The unfiltered implantation detector rate and gamma rate was built. Using the uncorrected rates as an input, the gamma detector rate was corrected for bin by bin. The correction used is shown in equation 6.1

$$r^c_{coincidence} = \frac{1}{1 - r_\beta \tau_\beta} \frac{1}{1 - r_\gamma \tau_\gamma} r^m_{coincidence} \tag{6.1}$$

where $r^c_{coincidence}$ is the corrected gamma-beta coincidence rate, r_β the raw measured implant rate, τ_β the dead time of the implant detector, r_γ and τ_γ the raw measured rate and dead time for the CsI(Na) detector, and $r^m_{coincidence}$ the measured coincidence rate. Then, after corrected for the dead time, each cycle was added together relative to the last beam off. These stacked cycles were used to find the half life.

For high beam intensity runs (i.e. sets 4,5 and 7), the dead-time corrections had a size of 31 to 36 ms. For low beam intesity runs, (i.e. set 3) the dead-time correction changed the half-life by 6 to 8 ms. The values shown in this chapter are those with the dead-time

28

correction.

Once the decay spectra were put in coincidence and stacked up, it was fit with equation 6.2

$$f(t) = a \exp\left(-t * ln2/T_{\frac{1}{2}}\right) \tag{6.2}$$

where a and $T_{\frac{1}{2}}$ are free parameters. a is the initial rate and $T_{\frac{1}{2}}$ the half-life. The decay curves were fit from 1.5 seconds past the beam on time to 1.5 second from the end of the decay time. The fitting method used was the log likelyhood method. The 60 second decay run up detector result is shown in Figure 6.10. From this run, it is seen that the spectra does not decay back down to the background. The lack of background parameter in equation 6.2 comes from this observation.

The decay spectra were built run by run, and the resulting fitting results were averaged together. Runs with a p-value less than 0.05 were considered statistically insignificant and thrown out. After all the significant half-lives were collected, the average of them all was taken.

6.3 Systematic Effects

Several systematic effects were looked at. The dead time correction was applied before any other systematics were investigated.

6.3.1 Dead Time

The timing resultion of the clock is 8 ns. Due to this, there is an uncertainty on the dead times of at least 8 ns. The dead times were varied ± 4 ns and the half lives calcluated. Half
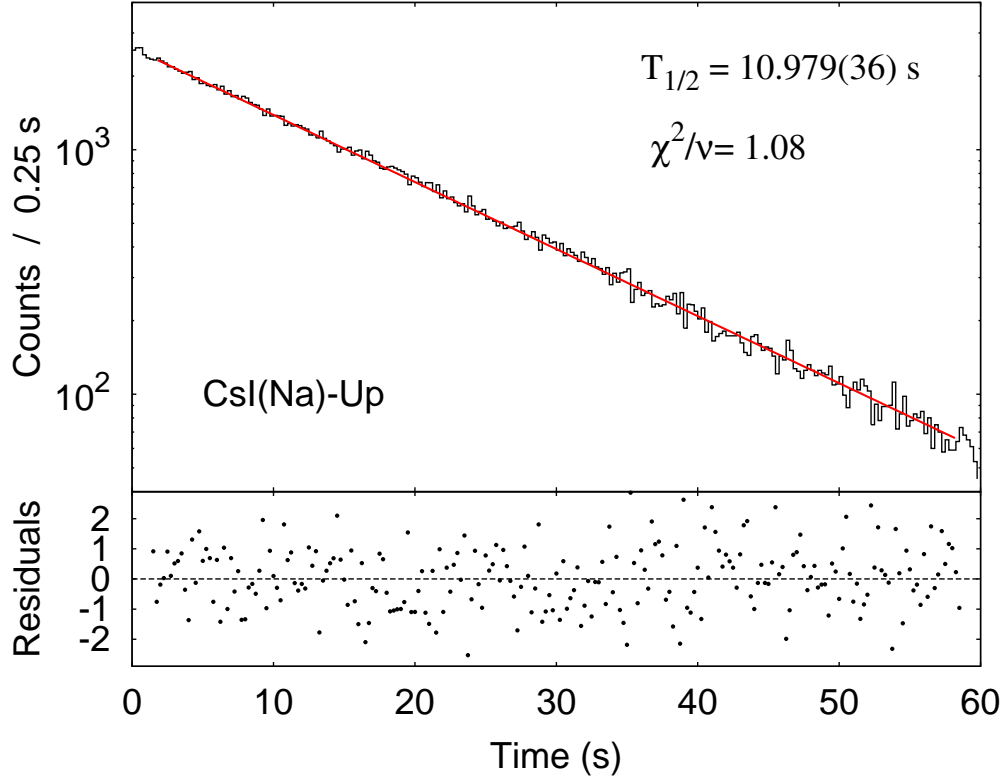
Figure 6.10: The decay spectrum from the up gamma detector is shown on the top graph. The red line is the exponential fit. The bottom graph shows the residuals from the fit.

the difference of those half lives is the systematic uncertainty.

6.3.2 Pile Up Effects

The dead time is overcorrected. Due to pile up, some of the pile up events are not totally lost. Some of the events thought to be missing just got shuffled around. This is a problem due to the fact that energy gates are imposed. The pile-up events also have a different time structure than the regular events. Due to the fact that the pile-up goes as the singles rate squared, the half-life of the pile-up events is half that of the non-piled-up events. This creates a background with a different time signature, and causes a change in half-life.

The 48 ns time cut around the peak, shown in Figure 6.7, was compared to several other,

larger time cuts. The narrow time cut still have some uncorrelated background and pile-up events in them.

To account for this effect, several other time cuts were taken. These cuts were plotted vs half-life. This graph was fit with a quadratic function. This function was extrapolated to zero, which was the correction due to the pile-up. This graph is shown in Figure 6.11.
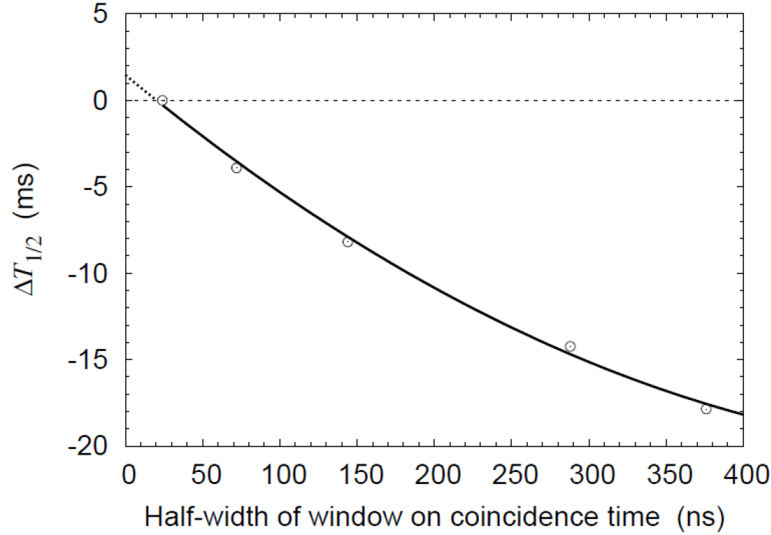
Figure 6.11: Time difference vs the resulting half-life. The line is a quadratic fit which was extrapolated to zero.

The extrapolation line is shown. The half-life was corrected to the zero value of the window. The difference between this extrapolated value and the previously measured value was taken as a correction and as an error bar.

6.3.3 Background

The first systematic effect is the effect of background. Due to the low decay time, directly fitting a background is impossible. There is no background region for the fitting function to anachor to, which induces a large correlation between the background and the half life. Several techniques were used to estimate the background.

6.3.3.1 Simultaneous vs Seperate Fitting

The first attempt was by simultaneously fitting each run with a different fitting function. The equation used was equation 6.3.

$$f(t) = a(\exp -t * ln2/T_{\frac{1}{2}} + b) \tag{6.3}$$

with a and $T_{\frac{1}{2}}$ the same as in equation 6.2 and b the relative background level. The half-life of the four detectors was set to be a common parameter. The relative background level and initial rate, however, were assumed to be independent for each spectrum. The resulting half life was compared to the value found with fitting each detector seperately without a background.

The effect of adding a background was investigated using Monte Carlo. Exponentials were generated and an ammount of background added. The resulting function was fit with a decay curve without a background parameter. The amount of background added was varried, and the resulting half lives plotted. It was found that increasing the background decreased the value of the half life, and that the background level and the half life value were strongly correlated.

A similar Monte Carlo was written to check the simultaneous fit method. Four decay curves were fitting and simultaneously fitted the same way was the data. They were also fitted seperately with only an exponential decay. The background was varied and the difference between the two values was taken. The method shows a trend similar to the one seen in the previous Monte Carlo.

In the data, it was discovered that the results of the simultaneous vs seperate fitting depended on the size of the dead time correction. If the dead time was overcorrected, it

induced an effect that was similar to having a larger background. If more dead time was imposed, the effect was as if there was a negative background. A dead time correction was added to the Monte Carlo, and a similar trend was seen. As long as the dead time is known exactly, the background can be extracted with this technique. However, as it is somewhat uncertain of what the exact dead time should be, this technique cannot be used to determine the background.

6.3.3.2 Spectra Arguments

The other way to try and gauge the background size is to look at the spectra. Looking at Figure 6.7, it can be seen that on the left side of the large peak, there are very few counts. It can also be seen that the prompt peak in the center contains most of the counts, while there is a long tail on the right side of the peak. This tail is due to pile up. An event in the beta window piles up with another event later in time. The second event is read by a gamma detector, but is correlated with the first event, causing the large time difference. The time spectrum changes if the beta spectrum is cut in different ways.

In the gamma beta spectrum, it can be seen that there is no background events aside from the 511 region. This is due to the presence of ^{10}C and ^{11}C. When the detectors are put into tripple and quadruple coincidence, the gamma rays of those isotopes appear. There are no gamma rays in the 1620 keV window which was filtered on.. The only coincidence possible is if there is pile up into that window along with a beta event. The estimate of those events is shown on the left side of the peak in the time difference figure shown in Fig. 6.7 These events are accounted for when extrapolating the different time difference cuts, as shown in Figure ??

6.3.4   Cut Sensitivity

For each pair of detectors, there were four conditions: two for each the implant and gamma detectors. For the gamma cuts, the edges of the gates were varied $\pm$ 5 keV in each direction for each cut. The results is insenitive to the upper beta cut. The lower beta cut was scanned with 6 different values going evenly from the initial lower beta cut to the peak of the spectrum. Moving the lower beta cut also effects the dead time correction. In order to disentangle the two, the lower beta cut was varied with two different time difference conditions. The location where the difference between the two calculations blows up is where the effect of the lower beta cut starts being swamped by the effect of the pile up. This is limit of where the lower beta cut was scanned. All four of these conditions were varied independently, and the procedure of generation the spectrum and fitting the decay curves was done. Half the resulting range of half-life values was taken to be a systematic uncertainty.

The fitting range of the decay spectra was varied. The start of the fit was varied bin by bin up to 6.5 seconds into the decay spectrum. The end of the fit was varied the other way to cut out the end of the decay spectrum. Since there was no noticable systematic effect, there was no increase in error associated with this effect.

6.3.5   Oscillator Stability

The oscillator of the PIXE board has a stability of $\pm 5 * 10^{-5}$. All times in the analysis were stretched by this value, and the half life calculated. Have the difference between the stretched value and the original value is another systematic error.

6.3.6 Binning and Fitting

In order to check the senstivity of the result to binning, the decay curves were rebinned by a factor of two. Half the difference between the rebinned half life and the original half life is considered the correction and the uncertainty.

For the fitting method, log-likelihood estimators were used to fit the summed data. This was done with two different packages which gave identical results. This was compared to analytic results, which gave the same results, so the half life is insensitive to the fitting method.

6.4 Result and discussion

The PVT runs are shown in Figure 6.12

The results for the PVT runs are shown in in table 6.2 for the PVT runs.

Table 6.2: The PVT runs

Detector	Half-Life	Error
Up	11.0195	0.0088
Left	10.9944	0.0087
Down	10.9980	0.0085
Right	10.9987	0.0095
Mean	10.9999	0.0044

The size of the systematic errors investigated are shown in table 6.3

After the dead time correction, the value of the half-life from the CsI(Na) implant detector runs was found to be 11.0011 ± 0.0069 (stat) ± 0.0030 (syst) s.
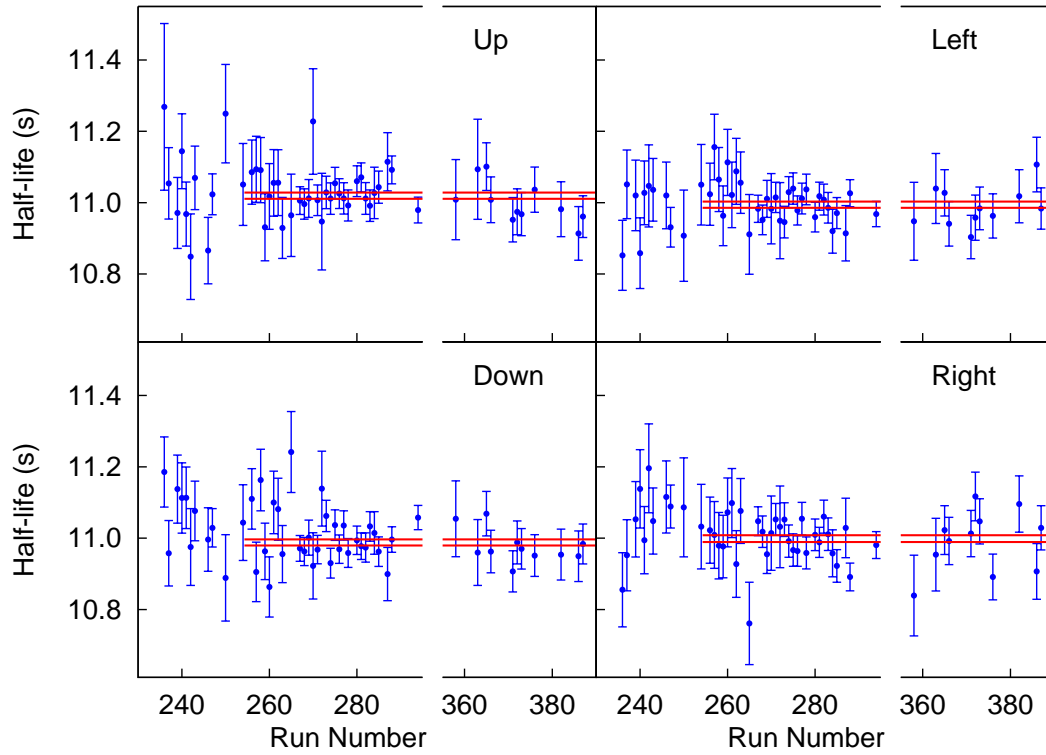
Figure 6.12: The red lines show the results of the fits over the runs that were used. The additional half-lives shown are excluded to reasons discussed previously.

Table 6.3: Systematics

Source	Correction [ms]	Uncertainty [ms]
Dead-time	0.00	0.24
Oscillator stability	0.00	0.80
Lower PVT cut	0.00	2.32
Lower gamma cut	0.00	0.15
Upper gamma cut	0.00	0.05
Uncorrelated events	1.47	1.47
Binning	-0.30	0.30
Total systematic	1.17	2.89

6.5 Conclusion

The half-life measured is most consistent with some previous measurements of a half-life of about 11 s. This can be seen in Figure 6.13. This measure disagrees with the most recent
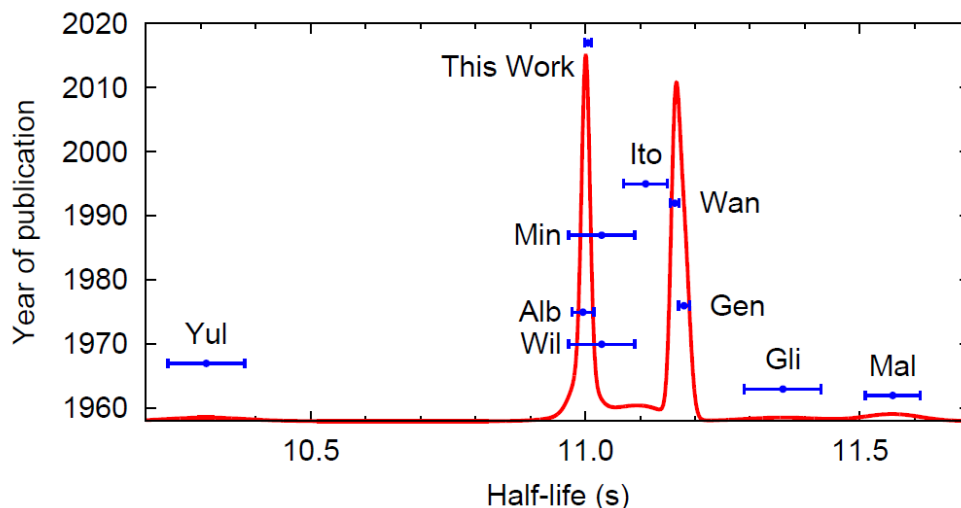
measurements.

Figure 6.13: A scatter plot of (a) previous values with this work added. The labels correspond to: Mal [6], Gli [4], Yul [14], Wil [13], Alb [1], Gen [3], Min [7], Wan [11] and Ito [5].

Several things about the data set were discovered. It was learned that there were contaminates coming from the fragmentation of the ^{12}C in the plastic scinttilator. The beta decaying products could be a cause of why the beta spectrum for the PVT detector looks so odd. It was also discovered that the rate dependent gain effect in the CsI(Na) implant detector is significant. Before doing this measurement, it was assumed that the low rates would make that effect negligable. It was learned that after the coincidence, the amount of background left in the spectrum is negligable, and that we have no contaminates in the beam.

Chapter 7

Fitting Beta Spectrum

In order to get a measurement of the Fierz term, the spectrum shape needed to get fit. The effect of bremstrahlung and the effieciency of the detectors needed to be accounted for. The way this was done was with a a simulation.

7.1 GEANT4 Monte Carlo

The corrected beta decay spectrum was fed as input to a Monte Carlo. The program used to model the detectors was GEANT4. In order to use the program, parameters must be introduced.

7.1.1 Detector Simulation

The geometry of the detector set-up was programmed into the simulation. The implant detector was modeled as a square prism of CsI. The rectangular prism was 9.76 cm deep with a 5 cm square base. The front edge implant detector was put at the center of the simulation. The aluminum sheath and MgO layer was not simulated for the implant detector.

The four large gamma detectors also square prisms. The active volume was 79.5 mm square and 76.2 mm deep. It was also made of CsI. Around this detector, a 1.5 mm laywer of MgO was added. On top of this, the can of aluminum, 1 mm thick, was added into the

simulation.

The four large gamma detectors were arranged into a square around the implant detector. Each square base of the gamma detectors was centered one inch upstream from the face of the implant detector. This modeled how the implant detector was recessed in the experiment.

7.1.2 Source Definition

The next step was to define a region inside the implant detector. This region was where the gamma and beta particles orignated from. The depth of the region was calculated using LISE++, a ion optics code. The verticle and horizontal size of the region was calulated by using the PPAC measurement and an ion optics simulation. This size was 0.4 mm deep, 3.5 mm wide, and 3.6 mm tall. The source was implanted 1.156 cm into the detector.

Once these parameters were known, GEANT4 was told to generate two particles. First, the corrected beta energy spectrum was sampled and an electron of that energy was generated inside the implant region. The beta energy spectrum was generated using all the corrections described in chapter (COME BACK TO THIS). The location of the electron was recovered, and a photon with an energy of 1.6 MeV was generated as well. The initital direction of the two particles was as isometric. These particles where then propagated through the detector setup.. GEANT4 uses a physics list that has all the interactions a particle could take. The physics list used was standard option 4. This list is better at low energy electron physics.

7.1.3 Primary Particle Definitions

There were three primary particles generated. Two were photons and one was an electron. All three particles had an isotropic angular distribution. The origin points of all the primary

particles was the same.

One photon was the 1.6336 MeV photon from the ^{20}F decay. The energy of this photon was not changed.

The electron was generated according to phase space spectrum (equation 2.3) times all the corrections. For the radiative correction, the electron was generated with the formala that assumes all real photon energy is absorbed (equation **??**). However, this is not exactly true. In this case, due to the geometry, photons are absorbed totaly if they are below 100 keV in energy. In order to properly see the effect of the real photon emmission, the second primary particle is used.

After the electron energy is generated, a formula describing the energy spectrum of the inner bremsstrahlung photons is generated. This spectrum is written out in equation **??**. Further discussion of this formula is found in the theory chapter. A cutoff of 50 keV is imposed to the formula, as it has a singularity at zero photon energy. Then, the formula is numerical integrated from 50 keV to the electron energy. This is the total probablity that an electron emits a KUB photon. This number is compared to a random number from 0 to 1. If the random number is below the integral, the inner bremsstrahlung energy spectrum is sampled. The algorithm used for this sampling is the van Neumann method [10]. The sampled energy is given to the third primary particle. The energy of the electron is reduced accordingly.

After all three particles have their energies defined, they are propogated through the detector set up.

7.1.4   Simulation Results Processing

The particles were tracked and the energy deposited in each detector summed up. The energy deposited in the implant detector was further seperated into two parts: Energy from the electron and the inner bremstrahlung photon. Energy from the 1.6336 MeV photon After the energies of the particles reached a certain threshold, the simulation of one decay was finished. All the energies deposited into each of the detectors was summed up and saved as an event in a ROOT tree. Then, the process was repeated. A new location inside the region was generated and another decay generated.

In order to get to get the necessary statistics, $2 * 10^9$ events had to be generated. After the events were done, the simulation data was processed further. Much like the experimental data, the simulated data had to be filtered. The energy absorbed in the implant detector was filtered by the energy absorbed in the outer four gamma detecters in the simulation.

The filtered data was seperated into two parts: Absorbed energy in the implant detector only orginating from the electron. Absorbed energy in the implant detector with some contribution from the gamma ray. These energies were built into two different histograms. These two histograms had the detector resolution applied to it.

The convolution function was

$$\sigma = A\sqrt{E} \tag{7.1}$$

where σ was the energy resolution, E the energy, and A a constant found through a calibration. After all histograms were convulted, they were ready to fit.

7.2 Calibration

In order to properly fit the energy spectrum, a calibration of the CsI(Na) detector had to be done. Several different energy lines were used to find the calibration and the energy resolution function. The lines were the 1.173228 MeV and 1.332.492 MeV gammas from a ^{60}Co source, the 0.661657 MeV gamma ray from a^{137}Cs source, and the 0.511 MeV and 1.274527 MeV gamma rays from a ^{22}Na source. These gamma rays were fitting with a gaussian and a background. The background varried from a linear background, a quadratic background, and an error function background. For the ^{60}Co, both peaks were fit at once. These different background gave slightly different results for the centroids and the widths of the gaussians. The different widths and centroids were taken as a systematic error. From the centroids, the calibration for each detector was calculated as:

$$C = G * E + b \tag{7.2}$$

where C is the location of the peak in ADC channels, G the gain in channels/keV, and b the offset in channels. The widths of the peaks were calibrated with the gain and plotted vs energy. Then, equation 7.2 was fit to the results in order to determine A.

7.3 Fitting Procedure

The simulation described above were only part of what was needed. Other simulations included in the fit had the phase space times corrections times or divided an additional factor of the total energy of the electron. The simulations were all convoluted and filtered as described above. The various simulations were taken together and the fit using the ROOT

algorithm.

I NEED TO EXPLAIN BETTER

BIBLIOGRAPHY

BIBLIOGRAPHY

[1] D. E. Alburger and F. P. Calaprice. Half-lives of ^{18}Ne and ^{20}F. *Phys. Rev. C*, 12:1690–1691, Nov 1975.

[2] I. Angeli and K. P. Marinova. Table of experimental nuclear ground state charge radii: An update. *Atomic Data and Nuclear Data Tables*, 99:69–95, January 2013.

[3] H. Genz, A. Richter, B.M. Schmitz, and H. Behrens. Half-life, endpoint energy, t value and shape factor in the decay of 20f. *Nuclear Physics A*, 267:13 – 28, 1976.

[4] S. S. Glickstein and R. G. Winter. Properties of f^{20}. *Phys. Rev.*, 129:1281–1283, Feb 1963.

[5] S. Itoh, M. Yasuda, H. Yamamoto, T. Iida, A. Takahashi, and K. Kawade. Measurement of Beta-decay Half-lives of Short-lived Nuclei by Using High-rate Spectroscopy Amplifier. In *1994 Symposium on Nuclear Data*, Tokai, Japan, March 1995.

[6] S Malmskog and J Konijn. Half-life measurements of 6he, 16n, 19o, 26f, 28al, 77senm and 110ag. *Nuclear Physics*, 38:196 – 210, 1962.

[7] Tadanori Minamisono. Nmr of short-lived nuclei implanted in crystals and a new isol for projectile fragments in relativistic heavy-ion reaction. *Hyperfine Interactions*, 35(1):979–991, Apr 1987.

[8] B. Pfeiffer, K. Venkataramaniah, U. Czok, and C. Scheidenberger. Atomic mass compilation 2012. *Atomic Data and Nuclear Data Tables*, 100(2):403 – 535, 2014.

[9] D.R. Tilley, C.M. Cheves, J.H. Kelley, S. Raman, and H.R. Weller. Energy levels of light nuclei, a = 20. *Nuclear Physics A*, 636(3):249 – 364, 1998.

[10] John von Neumann. Various techniques used in connection with random digits. pages 36–38, 1951.

[11] T.F. Wang, R.N. Boyd, G.J. Mathews, M.L. Roberts, K.E. Sale, M.M. Farrell, M.S. Islam, and G.W. Kolnicki. Measurement of the half-life of 20f. *Nuclear Physics A*, 536(1):159 – 167, 1992.

[12] D. Weisshaar, A. Gade, T. Glasmacher, G.F. Grinyer, D. Bazin, P. Adrich, T. Baugher, J.M. Cook, C.Aa. Diget, S. McDaniel, A. Ratkiewicz, K.P. Siwek, and K.A. Walsh. Caesara high-efficiency csi(na) scintillator array for in-beam ray spectroscopy with fast rare-isotope beams. *Nuclear Instruments and Methods in Physics Research Section A:*

Accelerators, Spectrometers, Detectors and Associated Equipment, 624(3):615 – 623, 2010.

[13] D. H. Wilkinson and D. E. Alburger. Mirror symmetry in the β decay of the $a = 20$ and 25 systems. *Phys. Rev. Lett.*, 24:1134–1136, May 1970.

[14] D.H. Wilkinson. Evaluation of beta-decay: I. the traditional phase space factors. *Nuclear Instruments and Methods in Physics Research Section A: Accelerators, Spectrometers, Detectors and Associated Equipment*, 275(2):378 – 386, 1989.

[15] Herbert P. Yule. Half-lives of some short-lived radioactive isotopes. *Nuclear Physics A*, 94(2):442 – 448, 1967.